Energetic Cavitation Collapse Generates 3.2 Mbar Plasma with a 1.4 J Driver

Marc C. Ramsey and Robert W. Pitz

Department of Mechanical Engineering, Vanderbilt University,
VU Station B #351592, 2301 Vanderbilt Place, Nashville, Tennessee 37235-1592, USA

(Received 28 November 2012; revised manuscript received 27 February 2013; published 10 April 2013)

A tabletop device uses 1.4 J to drive the symmetric collapse of a 1.8 mm radius vapor bubble in water at 22 bar. Single shot streak imaging reveals a stagnation plasma of 28 micron radius at over 12 000 K and an unprecedented pressure of 3.2 Mbar. Compared to sonoluminescence, the most commonly studied cavitation mechanism, this event is greater by factors of 30–40 in size, 1 000 000 in energy, and 100 in stagnation pressure. This regime of high energy density has previously been accessible only in massive facilities with very low repetition rates.

DOI: 10.1103/PhysRevLett.110.154301 PACS numbers: 43.25.+y, 47.40.Nm, 52.50.Lp, 78.60.Mq

Energy focused by the spherical collapse of a cavitation bubble can generate thermodynamic extremes at stagnation [1–3]. This phenomenon is commonly studied in the context of single-bubble sonoluminescence (SBSL) [4–7], where a bubble of about 50 μm maximum radius is driven periodically by an ultrasonic standing wave of 1–2 bar in amplitude. Each collapse has about 50 nJ of kinetic energy and proceeds to roughly 1 μm radius before emitting a picosecond burst of light [8–10], with the stagnation state estimated at 1–60 kbar [11–13] and 10^4–10^6 K [14–17]. However, the true stagnation mechanisms and state are debated [5–21], and SBSL cannot be readily scaled for practical study or application. SBSL is subject to strict limitations in parameter space enumerated carefully by Brenner *et al.* [6]. These stem from the fact that SBSL is fundamentally periodic; a single bubble oscillates in quasiequilibrium, so all phases of the cycle must be stable. Above a certain threshold of stagnation energy density, the bubble always disintegrates on rebound due to the Rayleigh-Taylor inertial instability when the low density bubble interior accelerates the liquid [22]. Ultimately, the same limitation applies to variants of SBSL which employ modified drive waveforms [23–28] or reduced frequency [29,30] to achieve larger or brighter events, but not a quantified increase in energy density. Nonperiodic cavitation mechanisms driven by laser breakdown [31,32] or plane-wave compression [33] avoid this limitation but sacrifice symmetry, which likewise limits the ultimate energy density.

We outline here a simple theory [1,6,22] of energetic cavitation collapse (ECC) designed to maximize energy focusing at arbitrary scale. A spherical bubble of radius $R = R_0$ is initially stationary in an infinite liquid with uniform density ρ_0 and temperature T_0. The bubble contains vapor at pressure $p_{V0} = f(T_0)$ and noncondensable gas at pressure $p_{G0} \ll p_{V0}$. This bubble is then driven to collapse by a step increase in far-field liquid pressure to some large value $p_\infty^* \gg p_{V0}$. The collapse energy is equal to the work done on the collapsing cavity $E = (4\pi/3){R_0}^3 p_\infty^*$. The collapse time is $t_{TC} = 0.915(\rho_0 {R_0}^2/p_\infty^*)^{1/2}$. A stagnation event brings the collapse to a halt when the interior pressure becomes comparable to the inertial forces.

The entire bubble radius evolution of even very energetic collapses can be modeled accurately by the theory of Gilmore [3]. However, here it is simpler to divide the collapse into distinct regimes: acceleration, incompressible coasting, transition, compressible coasting, stagnation, and shock emission. Acceleration occurs while the bubble radius proceeds from R_0 to $R_0/3$ (losing 96% of its volume). The applied pressure does work on the bubble and the energy of the fluid flow increases. This is followed by incompressible coasting, where the total kinetic energy is roughly constant and the liquid can be assumed incompressible. Total kinetic energy [1] is given by $E = 2\pi\rho_0(dR/dt)^2R^3$ and the bubble radius by $R_i = (E/\rho_0)^{1/5}(t_i - t)^{2/5}$ (subscript i denotes incompressible). Then there is a transition phase where the liquid compressibility becomes increasingly significant. Once the fully developed compressible flow is established [2] the bubble radius is given by $R_c = A_c(t_c - t)^{n_c}$ (subscript c denotes compressible). For water, Hunter [2] finds that $n_c = 0.555$ and A_c is a constant which depends on collapse energy. The stagnation event then occurs at a radius which depends on gas content and symmetry. Finally, a shock wave is emitted, shown by Hunter to have radius $R_s = A_s(t - t_s)^{n_s}$, where A_s and n_s are constants while the shock is strong (subscript s denotes shock). Each of these three forms includes a time offset (t_i, t_c, and t_s) which corresponds to a hypothetical instant of zero radius.

The sequence of events designed to approximate ECC and demonstrated here is as follows. (i) In degassed water held at its vapor pressure, a bubble is nucleated by near-threshold [34] laser breakdown. (ii) The bubble coasts to its maximum radius of ~2 mm in ~1 ms and contains primarily vapor. During this slow, decelerating growth, spherical symmetry is stabilized by inertial, viscous, and surface tension effects. (iii) Piezoelectric drivers supply a

symmetric pressure step function, driving the bubble to collapse. (iv) The collapse stagnates, emitting light for a few nanoseconds. (v) A strong shock carries away most of the collapse energy. (vi) The bubble disintegrates into a cloud of microbubbles on rebound. (vii) Continuously circulating fluid carries away the contaminating bubbles and the process can be repeated after about 20 sec.

The stainless steel vessel shown in Fig. 1(a) has an inner radius of 25 mm, four fused silica windows, and is filled with degassed, deionized, room temperature water. A closed continuous circulation and filtration system (not shown) eliminates contaminating microbubbles and maintains the pressure at or slightly below the vapor pressure (~ 2.3 kPa). A 1 mJ, 9 ns, 532 nm YAG laser pulse is focused at the vessel center with corrected optics ($f/1.3$) to nucleate a bubble with a few microjoules of kinetic energy. A total of 8 piezoelectric (PZT) stacks 10 mm in diameter and 60 mm in length penetrate the vessel via 16 mm diameter aluminum pistons. These PZT elements are energized with a 1000 V, 200 kW pulser, consuming 1.4 J of electrical energy. This generates a pressure rise of 22 bar at the vessel center with a 3 μs rise time and duration greater than 45 μs, as measured with a transducer (Kistler 601A).

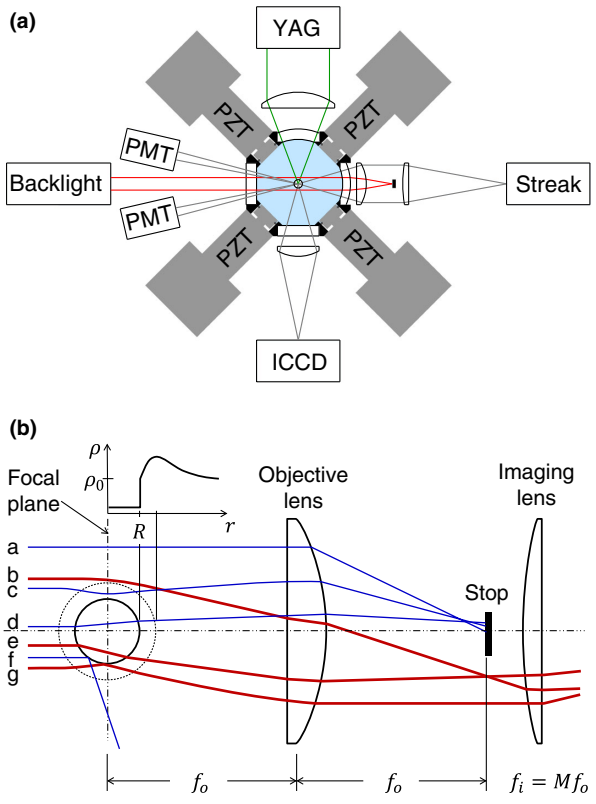

FIG. 1 (color online). A flattened top section view of the cavitation vessel (a) shows 4 of the 8 piezo (PZT) elements and diagnostics arranged for spatial streak imaging. Illustrative diagram (b) (not to scale) shows representative rays of the collimated backlight deflected by the bubble and density gradients [2] of the compressible collapse phase. The infinity corrected plan-apochromatic objective (numerical aperture 0.23) and imaging lenses have focal lengths (f.l.) f_o and f_i for magnification M, and resolve about 2 μm. The spherical-dome vacuum window is designed to be optically passive and is shown in (a) but not in (b).

The event is imaged onto a streak camera (Hamamatsu C7700) with a 100 mW, 660 nm collimated laser backlight. A central stop in the imaging system blocks weakly deflected rays as illustrated in Fig. 1(b). The stagnation location is monitored with a second intensified camera (ICCD). Two photomultiplier tubes (PMT, Hamamatsu R9880U) with 100 nm bandpass filters centered at 330 and 780 nm measure luminescence intensity and temperature with 1 ns resolution. A second 1 mW laser (not shown) partially blocked by the bubble provides a radius vs time signal used to anticipate stagnation and generate a trigger signal for diagnostics.

In an alternate configuration, the imaging optics were replaced with aluminum off-axis parabolic collection ($f/2$) and imaging (0.28 m f.l.) mirrors interposed by a fused silica dispersing prism. This spectrometer was calibrated with the known dispersion relation of fused silica, a HgAr atomic line lamp, and a calibrated deuterium-halogen broadband source (Avantes). The dispersion calibration was accurate to about 1 nm. The spectral sensitivity calibration is specified at $\pm 10\%$ overall, but local errors of up to 26% are suspected below 430 nm (see Fig. 4 caption).

Stroboscopic images of the final stages of an ECC event are shown in Fig. 2. These illustrate typical collapse symmetry, and show that low order shape perturbations grow slowly during collapse. Streak images are shown in Fig. 3. We focus our quantitative analysis on Fig. 3(b), which lies entirely in the compressible regime. The fitted parameter values are $A_c = 17.2 \pm 0.2\ \mu\text{m/ns}^{0.58}$, $n_c = 0.58 \pm 0.03$, $A_s = 19.2 \pm 0.2\ \mu\text{m/ns}^{0.68}$, and $n_s = 0.68 \pm 0.03$. The fits are not quite symmetric; these values represent an effective average. Other sources of uncertainty include spatial calibration (1%) and streak camera temporal calibration (less than 1%).

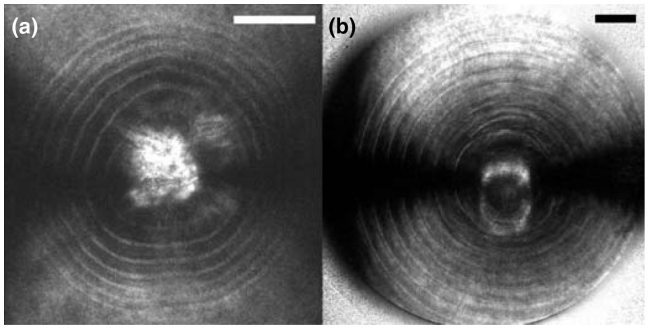

FIG. 2. Stroboscopic imaging backlit with 140 fs pulses at 80 MHz (12.5 ns interframe time) from a Ti:sapphire oscillator. The ICCD camera is gated to collect 8 superimposed exposures. The collapsing bubble (a) is primarily in the transition phase. The reflected shock and slowly rebounding bubble (of a different but similar event) are imaged in (b). Scale bars are 100 μm.

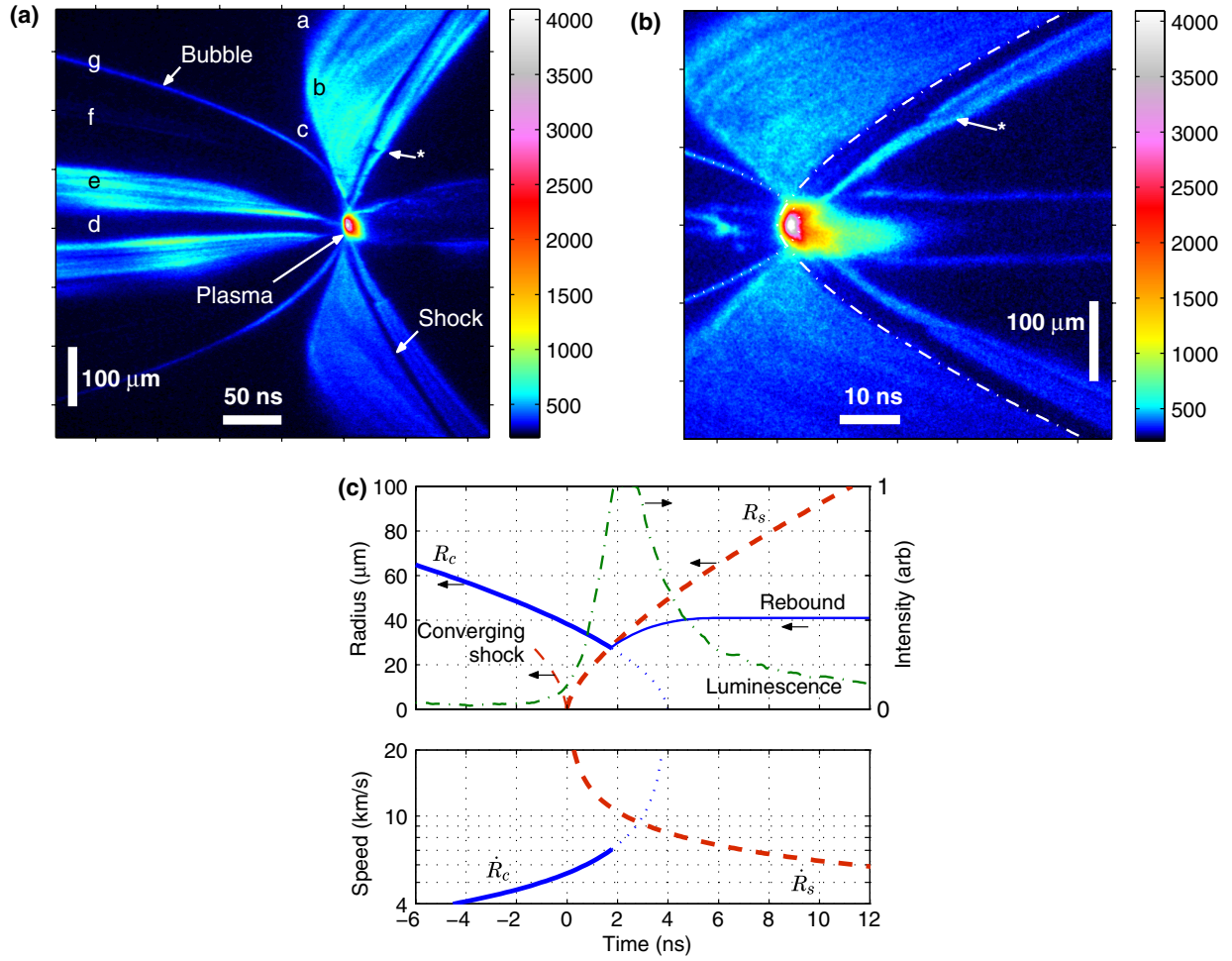

FIG. 3 (color online). A representative single shot spatial streak image which begins during the transition collapse phase (a) has regions labeled which correspond to the rays in Fig. 1(b). The bubble wall is accurately imaged by rays similar to g which are moderately deflected by total internal reflection from the bubble wall at glancing incidence. The density discontinuity at the reflected shock is opposite, so total internal reflection does not occur, and the shock appears in the image as a shadow where glancing rays are strongly refracted [not depicted in Fig. 1(b)]. Features illuminated by the low intensity laser backlight are rendered in "cold" colors (below 700 counts). The plasma emission can be distinguished by its far greater intensity, rendered in "hot" colors (1000–4096 counts). A similar image entirely in the compressible phase (b) has time resolution of about 1 ns. The bubble and shock radii are fitted with models R_c and R_s (white dotted and dash-dot lines). These fits are also shown in (c) along with the luminescence intensity at the bubble center. The zero of time is set to the hypothetical moment of zero shock radius t_s, which also corresponds with the onset (10% peak) of plasma emission. The hypothesized converging shock and bubble rebound are sketched for illustration.

Another error source which may be significant but is difficult to quantify is the deformation of the image as a result of refraction in the density gradients in the liquid near the bubble. We believe this error to be small due to conceptual analysis of Fig. 1(b) as well as the fact that bubble and shock motion appear consistent in data which span both compressible and incompressible phases and spatial regions (e.g., Fig. 3(a), along with data at much longer time scales, not shown). Quantification of this effect would be a major undertaking, and may be attempted in future work.

The event in Fig. 3(b) had a measured collapse time of $t_{TC} = 35\ \mu$s (the difference between known pressure pulse arrival and observed luminescence emission times) and energy of $E = 57$ mJ. (Energy was measured during incompressible coasting of similar events, standard deviation 1.5 mJ.) The calculated maximum radius and effective driving pressure for this collapse are then $R_0 = 1.8$ mm and $p^*_\infty = 22$ bar. The solution of the Gilmore theory at these parameters, when fit in the same way as the data, gives values of $A_c = 15.3\ \mu\text{m/ns}^{0.545}$ and $n_c = 0.545$. The small discrepancy with the measured values given above may result from the simplified equation of state for water employed by both Gilmore [3] and Hunter [2]. An estimate of the liquid pressure in the vicinity of the bubble based on the measured wall acceleration just before stagnation (1.4×10^{12} m/s^2) shows that it slightly exceeds 100 kbar, the validity limit of that state equation.

Figure 3(c) shows the bubble and shock fits R_c and R_s along with the plasma emission (luminescence) intensity at the centerline of the image. The bubble and shock intersect at a radius of 28 μm, bringing the collapse to a halt. The remainder of the bubble fit is unphysical (dotted). The apparent rise time of the plasma emission is roughly 1 ns, equal to the resolution of the measurement, and it begins before the bubble and shock intersect. In Fig. 3(b) it appears that the emission begins at the center of the bubble and propagates outward with time. From these observations we suggest that the plasma emission is initiated by the reflection of a converging shock as predicted by Wu and Roberts [18]. The presumed approximate form of the converging shock and the rebounding bubble are sketched in Fig. 3(c). (Neither is visible in the data, though the final quasistatic ~40 μm radius of the bubble is.) The existence of shock waves within the bubble is corroborated by the fact that here the parameter ϵ_p defined by Lin *et al.* [35] has a value at least ten times greater than in the cases considered there, due to the greater drive pressure [1].

Figure 3(c) also shows the velocity magnitude of the bubble wall and the reflected shock wave, which crosses into the liquid at 1.8 ns. At that instant, the liquid is moving inward at $R_c = 7$ km/s and the shock outward at $R_s = 11$ km/s, so the velocity of the shock relative to the upstream fluid is $u_s = 18$ km/s. The shock is unsupported by an energy source so it has the character of a blast wave [36] (shock compression followed immediately by a rarefaction), and the hot emitting plasma in the bubble interior quenches quickly after the shock enters the liquid. The shock nearly reverses the inward liquid flow, but the trailing rarefaction almost immediately decelerates it back to near zero in the lab frame. This is predicted by Wu and Roberts [18] and observed here by the nearly stagnant bubble radius after the wave passes. Unfortunately, the fluid velocity immediately behind the shock front is not directly measured. However, we may apply an approximate theory in the strong shock limit [36] since the ratio of preshock (~100 kbar) to postshock (~Mbar) pressure is roughly 10. The postshock pressure is then $p_s = \rho_0 {u_s}^2$ or 3.2 Mbar. A conservative lower bound for the shock pressure can be found from exact theory [36] by recognizing that the liquid flow is certainly arrested if not reversed, so the particle velocity $u_p \geq 7\,\mathrm{km/s}$. This lower bound is then $\rho_0 u_s u_p \geq 1.3\,\mathrm{Mbar}$.

The disturbance in the shock wave at about 25 ns after stagnation observed in both Figs. 3(a) and 3(b) (labeled *) may result from a second shock wave, also predicted by Wu and Roberts [18], which overtakes the first.

Figure 4 shows time-resolved luminescence emission spectra. (Measurements with the two PMTs yield results consistent with these.) The rise and fall times are slightly longer than in Fig. 3(c), probably as a result of reduced symmetry. (Symmetry could not be monitored while collecting spectral data.) Still, the temperature peaks very early in the event as the reflected shock forms. Intensity peaks later as the radiating shock propagates outward to larger radius. A peak temperature between 12 000 and 14 000 K is typical of all data at various collapse energies. Both temperature and intensity drop abruptly when the shock crosses the bubble wall into the cool liquid. A slow exponential decay in temperature and intensity follows.

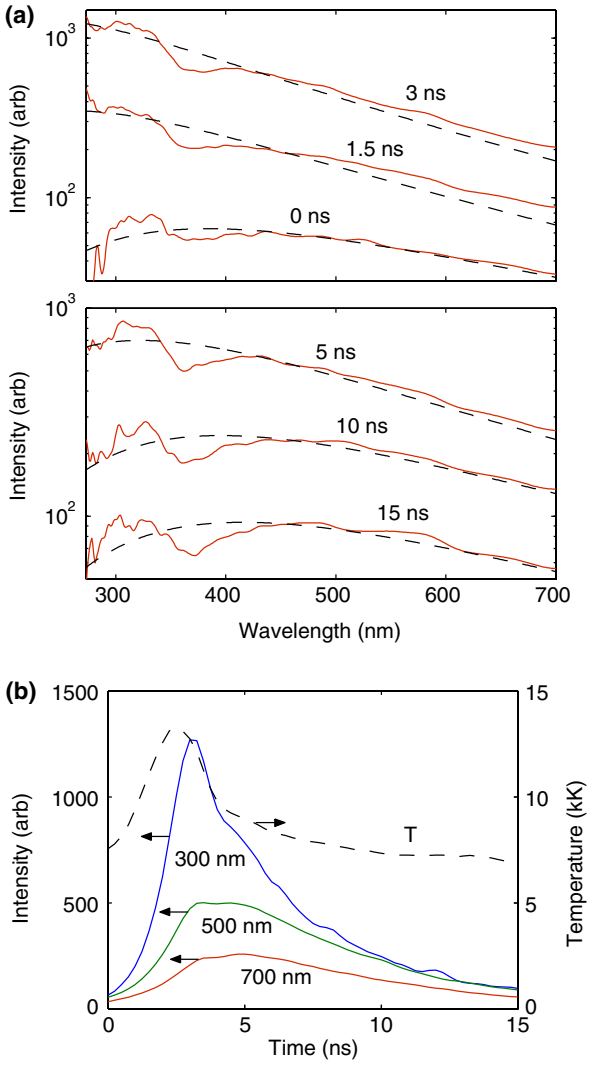

FIG. 4 (color online). Single-shot, time-resolved spectroscopy of the stagnation luminescence has resolution of about 1 ns. Zero time is defined at 10% peak intensity, so this time scale corresponds roughly to Fig. 3(c) (though it is a separate event). Instantaneous spectra (solid) at several times (a) are shown with blackbody fits (dashed). The raw spectral data (not shown) are very smooth; the obvious deviations from the fits at wavelengths below 430 nm result from known imperfections in the calibration provided by the manufacturer of the deuterium-halogen reference lamp. (b) Fitted blackbody temperature as a function of time, along with intensity at three representative wavelengths.

The plasmas generated here fall into the regime of high energy density known as warm dense matter, the

subject of active research in astrophysics and in the pursuit of inertial confinement fusion [36,37], and previously accessible only in massive facilities with low repetition rates [38–40]. ECC is well controlled, repeatable several times per minute, and accessible by detailed diagnostics. This type of event could be employed to investigate the equation of state of materials at high energy density, as well as the dynamics of spherical implosions relevant to inertial confinement fusion.

We thank L. Pickelmann at Piezomechanik GmbH and R. Keith and J. Case at KMW Inc. for fabrication, M. Cuneo, E. Yu, B. Atherton, M. Geissel, P. Rambo, and J. Schwarz at Sandia National Laboratories for helpful feedback and loan of a streak camera, and J. Valentine at Vanderbilt for use of a Ti:sapphire oscillator. Financial support provided by the National Science Foundation Graduate Research Fellowship (M. C. R.), Vanderbilt University, and Sandia National Laboratories. Sandia is a multiprogram laboratory operated by Sandia Corporation, a Lockheed Martin Company, for the United States Department of Energy's National Nuclear Security Administration under Contract No. de-AC04-94AL85000.

[1] L. Rayleigh, Philos. Mag. **34**, 94 (1917).
[2] C. Hunter, J. Fluid Mech. **8**, 241 (1960).
[3] R. Hickling and M. Plesset, Phys. Fluids **7**, 7 (1964).
[4] D. F. Gaitan, L. A. Crum, C. C. Church, and R. A. Roy, J. Acoust. Soc. Am. **91**, 3166 (1992).
[5] B. P. Barber, R. A. Hiller, R. A. Lofstedt, S. J. Putterman, and K. R. Weninger, Phys. Rep. **281**, 65 (1997).
[6] M. P. Brenner, S. Hilgenfeldt, and D. Lohse, Rev. Mod. Phys. **74**, 425 (2002).
[7] W. Lauterborn and T. Kurz, Rep. Prog. Phys. **73**, 106501 (2010).
[8] B. P. Barber and S. J. Putterman, Nature (London) **352**, 318 (1991).
[9] W. C. Moss, D. B. Clarke, J. W. White, and D. A. Young, Phys. Fluids **6**, 2979 (1994).
[10] B. Gompf, R. Gunther, G. Nick, R. Pecha, and W. Eisenmenger, Phys. Rev. Lett. **79**, 1405 (1997).
[11] R. Pecha and B. Gompf, Phys. Rev. Lett. **84**, 1328 (2000).
[12] K. R. Weninger, P. G. Evans, and S. J. Putterman, Phys. Rev. E **61**, R1020 (2000).
[13] D. J. Flannigan, S. D. Hopkins, C. G. Camara, S. J. Putterman, and K. S. Suslick, Phys. Rev. Lett. **96**, 204301 (2006).
[14] C. Camara, S. Putterman, and E. Kirilov, Phys. Rev. Lett. **92**, 124301 (2004).
[15] D. J. Flannigan and K. S. Suslick, Nature (London) **434**, 52 (2005).
[16] W. Chen, W. Huang, Y. Liang, X. Gao, and W. Cui, Phys. Rev. E **78**, 035301 (2008).
[17] D. J. Flannigan and K. S. Suslick, Nat. Phys. **6**, 598 (2010).
[18] C. C. Wu and P. H. Roberts, Phys. Rev. Lett. **70**, 3424 (1993).
[19] W. C. Moss, D. B. Clarke, and D. A. Young, Science **276**, 1398 (1997).
[20] S. Hilgenfeldt, Nat. Phys. **2**, 435 (2006).
[21] S. Khalid, B. Kappus, K. Weninger, and S. Putterman, Phys. Rev. Lett. **108**, 104302 (2012).
[22] C. E. Brennen, *Cavitation and Bubble Dynamics* (Oxford University Press, New York, 1995).
[23] W. C. Moss, D. B. Clarke, J. W. White, and D. A. Young, Phys. Lett. A **211**, 69 (1996).
[24] J. Holzfuss, M. Ruggeberg, and R. Mettin, Phys. Rev. Lett. **81**, 1961 (1998).
[25] J. L. Thomas, Y. Forterre, and M. Fink, Phys. Rev. Lett. **88**, 074302 (2002).
[26] J. L. Thomas, Phys. Rev. E **70**, 016305 (2004).
[27] T. Kurz, D. Kröninger, R. Geisler, and W. Lauterborn, Phys. Rev. E **74**, 066307 (2006).
[28] D. F. Gaitan *et al.*, J. Acoust. Soc. Am. **127**, 3456 (2010).
[29] C.-K. Su, C. Camara, B. Kappus, and S. J. Putterman, Phys. Fluids **15**, 1457 (2003).
[30] A. Chakravarty, T. Georghiou, T. E. Phillipson, and A. J. Walton, Phys. Rev. E **69**, 066317 (2004).
[31] O. Baghdassarian, B. Tabbert, and G. A. Williams, Phys. Rev. Lett. **83**, 2437 (1999).
[32] C.-D. Ohl, T. Kurz, R. Geisler, O. Lindau, and W. Lauterborn, Phil. Trans. R. Soc. A **357**, 269 (1999).
[33] B. Kappus, S. Khalid, and S. Putterman, Phys. Rev. E **83**, 056304 (2011).
[34] A. Vogel, K. Nahen, D. Theisen, and J. Noack, IEEE J. Sel. Top. Quantum Electron. **2**, 847 (1996).
[35] H. Lin, B. D. Storey, and A. J. Szeri, J. Fluid Mech. **452**, 145 (2002).
[36] R. P. Drake, *High Energy Density Physics* (Springer, New York, 2006).
[37] Y. B. Zel'dovich, and Y. P. Raizer, *Physics of Shock Waves and High-Temperature Hydrodynamic Phenomena* (Dover, Mineola, New York, 1966).
[38] A. H. Jones, W. M. Isbell, and C. J. Maiden, J. Appl. Phys. **37**, 3493 (1966).
[39] J. M. Soures *et al.*, Phys. Plasmas **3**, 2108 (1996).
[40] M. K. Matzen *et al.*, Phys. Plasmas **12**, 055503 (2005).